Improved sizing calculator for rapid optimisation of pack configuration at early-stage automotive product development

Thomas Grandjean
Energy and Electrical Systems, WMG
University of Warwick
Coventry, UK
T.Grandjean@warwick.ac.uk

James Taylor
Energy and Electrical Systems, WMG
University of Warwick
Coventry, UK
J.E.Taylor@warwick.ac.uk

Andrew McGordon
Energy and Electrical Systems, WMG
University of Warwick
Coventry, UK
A.McGordon@warwick.ac.uk

James Marco
Energy and Electrical Systems, WMG
University of Warwick
Coventry, UK
James.Marco@warwick.ac.uk

***Abstract*—The specifications that define a new automotive product development are established at an early stage in the product life cycle and define the direction of such a development, and changing these decisions becomes costlier the further the project evolves towards introduction into the market. Simulations and predictions underpin the crucial decisions made at the inception stage of the new product development life cycle, since these tools inform prototype development, production strategies, and improve profitability. The tool presented facilitates the decisions required when embarking on the new product development of a vehicle that incorporates electric-drive technologies and the vital choices made regarding the battery pack powering by such a vehicle. The tool functions can be split into two parts, firstly it incorporates a sizing model for determining the number of cells and the configuration required to meet a specified battery requirement. Secondly, a 1-D model is implemented to determine some of the basic thermal and power characteristics that can then be utilised to inform other parts of the design specification. Improvements are proposed that improve previous model accuracy from 8-9% to 6% for thermal predictions and down to 3% for electrical simulations. When integrated with a database containing cell characteristics, the tool can identify candidate cells that meet the proposed requirements. In addition, the tool's rapid execution time allows fact comparison between cell choices, at a level comprehensible by all project stakeholders in the decision making process.**

Keywords—Electric Vehicles, Hybrid Electric Vehicles, Batteries & Energy Storage, Design Tool, Thermal predictions

I. INTRODUCTION

When undertaking the development of a new electric automotive product, a set of initial requirements is established in order to best meet the needs of the potential market space, covering aspects such as performance, cost of manufacture, cost of use, lifespan, price point and many other factors of its design [1]. This underpins further requirement specifications such as sizing, technologies to use and other more engineering aspects of the initial design [2]. During the new product development, the engineering design evolves to include factors specific to the electric vehicle (EV) architecture: - drive trains, charging systems, power distribution systems, electric motors and batteries [3]. Amongst these, the battery is at the heart of the eventual performance of an EV product, governing factors such as range, lifespan and dynamic performance. The battery also represents a significant proportion of the product's total value [4], and its design can inform other aspects of system design such as thermal and electronic management systems.

In line with concerns over local air pollution [4], and legislation to reduce carbon emissions, such as the EU 2020 targets [5], electric vehicles have gained attention [6] as a solution to reduce the automotive industry's dependence on the internal combustion engine (ICE) [7]. Due to their long cycle life, slow self-discharge rates, high energy density, and lack of memory effect, Li-ion batteries are established as the predominant choice for new low carbon transport solutions [8].

Lithium ion batteries require organic electrolytes due to the wide operating voltage of the cell [9]. The electrolytes are based on combinations of linear and cyclic alkyl carbonates, which allow the use of lithium as the anodic active component and gives lithium ion batteries their high power and energy densities characteristics. However, these organic electrolytes have high flammability and volatility that pose serious safety issues as they can react with the active electrode materials to release significant heat and gas, such as carbon dioxide, vaporized electrolyte consisting of ethylene and/or propylene, and combustion products of organic solvents [9]. In addition to safety concerns, the temperature sensitivity of the conductivity of the organic electrolyte makes lithium ion battery properties, such as internal resistance, more temperature dependent than other types of batteries [10]. Consequently, there has been

considerable research into thermal modelling of lithium ion batteries [11, 12].

In automotive vehicles, lithium ion cells are expected to deliver large C rates, e.g. 1-5C and 10-20C in EV and HEV applications respectively. These C-rates cause the bus bar and contactors in pack and module assembly to generate heat, which needs to be considered by the battery thermal management systems in order to maintain the cells within their temperature operating window for safety and efficiency. Despite these essential pack and module components heating effects, most battery models only consider cell self-heating [13, 14]. In high current applications, such as automotive vehicles, the additional heat generated from these components cannot be neglected.

In order to improve thermal predictions, a sizing tool which only considers cell self-heating [15] is improved by considering heating from other components such bus bars and contactors. The sizing tool is comprised of two sub models. The first is a sizing model, which determines configuration and the number of cells necessary in order to meet a specified battery requirement. The second is a 1-D model, which is implemented in order to determine some of the basic thermal and power characteristics that can then be utilised to inform other parts of the design specification. The latter model is improved in order to improve thermal predictions.

II. Model Improvements

A full description of the models is given [15] and is not repeated in this article, a brief description of the 1-D model thermal is outline in this section. The 1-D thermal model has three cooling options in order to help inform which cooling strategy will be suitable for the application. The first strategy is no cooling. The second is active tab cooling, as shown in Figure 1.

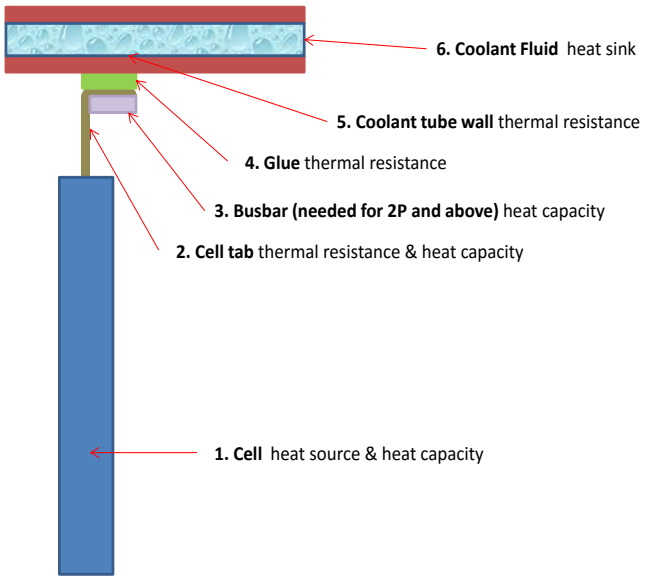

Figure 1. Active tab cooling

Figure 1 details the heat source (cell), heat capacities (cell, cell tab, and bus bar), thermal resistances (cell tab, glue, and coolant tube wall), and heat sink (coolant fluid) for the active tab cooling strategy. Finally, the third strategy is active cell surface cooling, as shown in Figure 2.

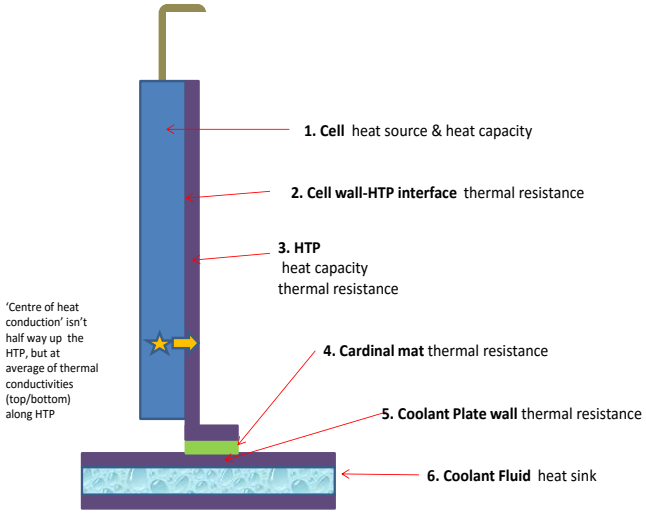

Figure 2. Active cell surface cooling

Figure 2 details the heat source (cell), heat capacities (cell and heat transfer plate - HTP), thermal resistances (cell tab wall to HTP interface, heat transfer plate - HTP, cardinal mat and coolant plate wall) and heat sink (coolant fluid) for the active cell surface cooling strategy. In Figure 2 the 'centre of heat conduction' is not half way up the HTP, but at the average of thermal conductivities (in the vertical orientation) along the heat transfer plate (HTP).

As depicted in Figure 1 and Figure 2, both active cooling strategies only have one heat source, i.e. the cell. This is also the case for the no cooling strategy. However, this will lead to underestimating the heat generation inside battery packs since there are other heat sources to consider, such as the bus bar, the battery management system (BMS), the contactors, and the wiring harness. These heat up due to Joule heating, i.e. the passage of an electric current through these conductive devices produces heat. The Joule-Lenz law states that the power loss through heat generation by an electrical conductor is proportional to the product of its resistance and the square of the current. Joule heating has a coefficient of performance of 1, i.e. every 1 watt of electrical power is converted to 1 Joule of heat. Therefore, the heat energy generated by Joule heating in watts, λ, is given by:

$$\lambda = I^2 Rt \tag{1}$$

Where I is the current in amperes flowing through the electrical conductor, R is the resistance in Ω of the conductor, and t is the time in seconds of the current. The resistance of the devices depend of their geometry and material composition. Assuming a totally uniform current density throughout the conductor, the resistance in Ω, R, is computed using:

$$R = \frac{\rho l}{A} \tag{2}$$

Where ρ is the electrical resistivity in Ωm of the material, A is the cross-sectional area in m^2 of the conductor, and l is the length in m of the conductor. The electrical resistivity, or specific electrical resistance, is a property of the material the conductor is made of. For example, bus bars are often made of copper or aluminium, which have an electrical resistivity of 1.68 x 10^{-8} Ωm at 20°C and 2.82 x 10^{-8} Ωm at 20°C respectively. The resistance of the contactors is given by the manufacturer stated value on the datasheet, e.g. the Gigavac high power contactor has max contact resistance of 0.4 mΩ.

III. Results

The model improvements are validated against a BMW i8 module. The module has a 16S1P configuration and is constituted of prismatic 20Ah cells. It has a terminal voltage of 56.7V and no active cooling.

The European Artemis (assessment and Reliability of Transport Emission Models and Inventory Systems) have developed chassis dynamometer procedures created by statistical analysis of a large database of European real world driving patterns. The CADC (Common Artemis Driving Cycles) include three driving schedules:

1. Urban
2. Rural road
3. Motorway

The first drive cycle, the high-power urban, is selected to be used for the validation since high transients caused the biggest challenge for model predictions. This section of the Artemis drive cycle determines the vehicle speed. The estimated resulting current applied to each individual cells is shown in Figure 3.

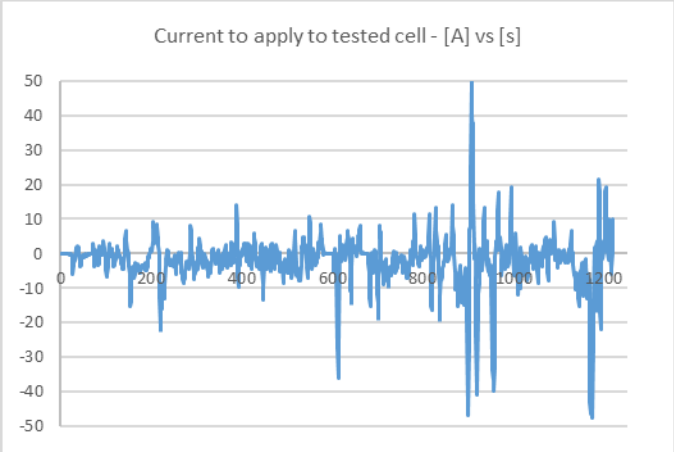

Figure 3. Validation drive cycle – current [A] vs time [s]

During the drive cycle, data is collected from eight thermocouples on the module surface. Thermocouples 1-6 are arranged around the module sides and thermocouples 7-8 are placed on top of the module packaging. The recorded module temperature from the eight thermocouples is shown in Figure 4.

The thermal results from the model, i.e. the battery back power, pack heat generated, and cell temperature rise are shown in Figure 5.

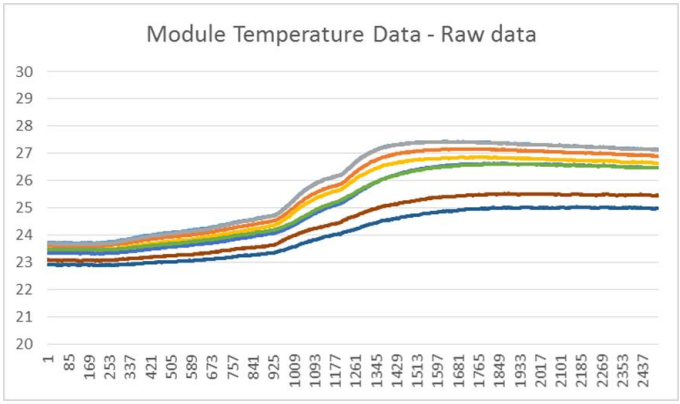

Figure 4. Module temperature data – temperature [°C] vs time [s]

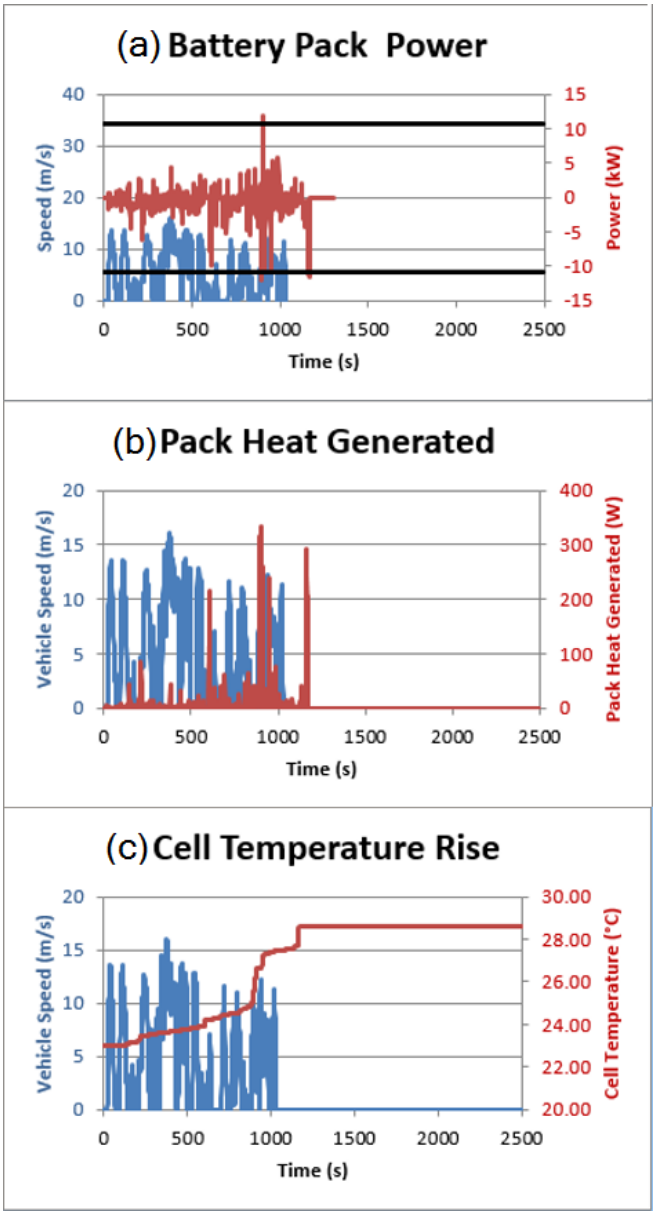

Figure 5. Thermal results: (a) battery pack power, (b) pack heat generated, (c) cell temperature rise.

In the previous version of the model, the pack heat generated was simply estimated by calculating the product of the pack current squared with the internal resistance of the pack. The latter is estimated by taking the manufacturer stated internal resistance value on the datasheet an individual cell and calculating the resulting pack internal resistance using the pack configuration (i.e. the number of cells in series and in parallel). In the improved version of the model, the pack heat generated shown in Figure 5(b) includes the heat generated from other devices, such as the bus bars and the contactors using (1) and (2).

The pack heat generated is used to calculate the temperature rise shown in Figure 5(c) based on the heat capacity of the pack, which is estimated by multiplying the number of cells by the manufacturer stated specific heat capacity value on the datasheet.

It can be seen from Figure 5(c) that the temperature is constant after the Urban section of the Artemis drive cycle. This is an intuitive result since there is no cooling in this validation and no more heat is being generated as the current is zero.

The real temperature measurements collected (Figure 4) are compared to model temperature predictions (Figure 5(c)) in order to validate the model improvements proposed. The average measured data and the model predictions are shown in Figure 6.

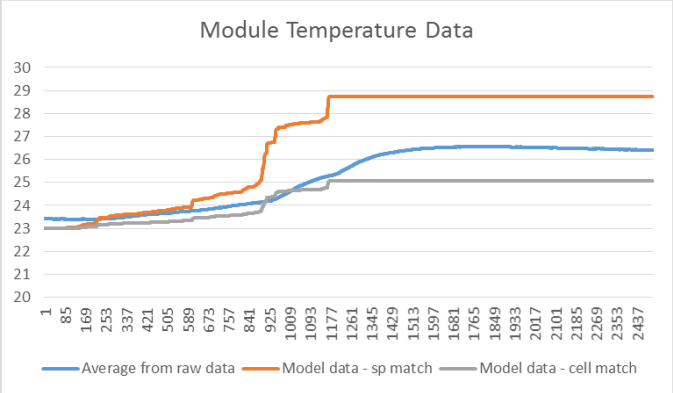

Figure 6. Module temperature validation – Temperature [°C] vs time [s]

Figure 6 shows good agreement between the model predictions and the average temperature collected. The difference between the average temperature of the eight thermocouples and the model temperature predictions is plotted as a percentage error in Figure 7. The worst case error, that is to say the difference between the coolest thermocouple (thermocouple 8), is also plotted on Figure 7.

Figure 7 shows there is a very good match to the thermocouples of the module sides (thermocouples 1-6) but a poor match when compared to the topside thermocouples (thermocouples 7-8), which are separated from the cells by the battery management system. The latter thermocouple couple positions are therefore cooler, as shown in Figure 4.

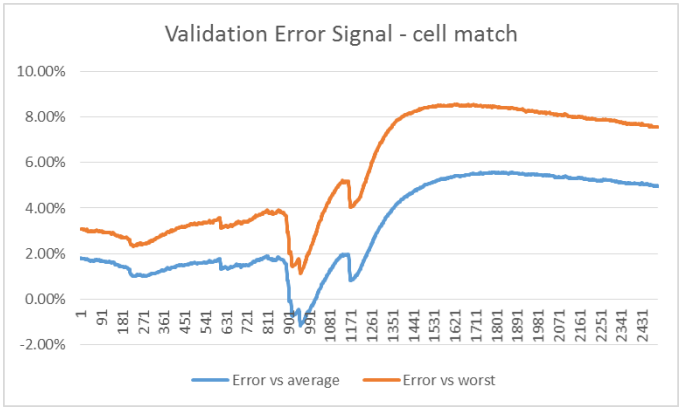

Figure 7. Cell temperature – Error [%] vs time [s]

The average error is 6.19%, which is an improvement when compared to using the previous version of the model (8-9% average error).

IV. Conclusion

A sizing tool previously published [15], was found to consistently underestimate battery pack prototype temperatures. Consequently, the thermal aspect of the sizing tool was improved in order to account for the heat generated by other essential battery components such as the bus bars and contactors. The improvements proposed are validated against a BMW i8 module and improve on previous model accuracy from 8-9% to 6% for thermal predictions and down to 3% for electrical simulations without significantly increasing the runtime. This allows for improved comparison between cell choices and cooling strategies and enables project stakeholders to make informed decisions at the inception stage of the new product development life cycle for future EVs.

Acknowledgment

The research presented within this paper is supported by the Innovate UK (https://hvm.catapult.org.uk/) through the WMG centre High Value Manufacturing (HVM) Catapult in collaboration with Jaguar Land Rover and TATA Motors.

References

[1] C. Wu, J. Wan, and G. Zhao, ‘Addressing human factors in electric vehicle system design: Building an integrated computational human–electric vehicle framework’, *J. Power Sources*, vol. 214, pp. 319–329, 2012.

[2] S. C. Nagpure, R. Dinwiddie, S. S. Babu, G. Rizzoni, B. Bhushan, and T. Frech, ‘Thermal diffusivity study of aged Li-ion batteries using flash method’, 2010.

[3] P. A. Cassani and S. S. Williamson, ‘Feasibility Analysis of a Novel Cell Equalizer Topology for Plug-In Hybrid Electric Vehicle Energy-Storage Systems’, *IEEE Trans. Veh. Technol.*, vol. 58, no. 8, pp. 3938–3946, Oct. 2009.

[4] J. H. Seinfeld and S. N. Pandis, *Atmospheric chemistry and physics : from air pollution to climate change*. Hoboken, NJ, USA: John Wiley & Sons, 2016.

[5] The European Parliament and the Council of the European Union, ‘Regulation (EU) No 333/2014 of the European Parliament and of the

Council of 11 March 2014 Amending Regulation (EC) No 443/2009 to Define the Modalities for Reaching the 2020 Target to Reduce CO2 Emissions From New Passenger Cars', *Off. J. Eur. Union*, vol. L103, pp. 15–21, 2014.

[6] H. Lund and W. W. Clark Ii, 'Sustainable energy and transportation systems introduction and overview', *Sustain. Energy Transp. Syst*, vol. 16, pp. 59–62, 2008.

[7] K. G. Høyer, 'The history of alternative fuels in transportation: The case of electric and hybrid cars', *Util. Policy*, vol. 16, no. 2, pp. 63–71, 2008.

[8] K. E. Aifantis, S. A. Hackney, R. V. Kumar, and Wiley InterScience (Online service), *High energy density lithium batteries : materials, engineering, applications*. Hoboken, NJ, USA: John Wiley & Sons, 2010, 2010.

[9] Q. Wang, P. Ping, X. Zhao, G. Chu, J. Sun, and C. Chen, 'Thermal runaway caused fire and explosion of lithium ion battery', *J. Power Sources*, vol. 208, pp. 210–224, 2012.

[10] S. Al Hallaj, H. Maleki, J. S. Hong, and J. R. Selman, 'Thermal modeling and design considerations of lithium-ion batteries', *J. Power Sources*, vol. 83, no. 1, pp. 1–8, 1999.

[11] X. Zhang, 'Thermal analysis of a cylindrical lithium-ion battery', *Electrochim. Acta*, vol. 56, no. 3, pp. 1246–1255, 2011.

[12] T. Waldmann, S. Gorse, T. Samtleben, G. Schneider, V. Knoblauch, and M. Wohlfahrt-Mehrens, 'A Mechanical Aging Mechanism in Lithium-Ion Batteries', *J. Electrochem. Soc.*, vol. 161, no. 10, pp. A1742–A1747, Jul. 2014.

[13] K. E. Thomas, J. Newman, and R. M. Darling, 'Mathematical Modeling of Lithium Batteries', in *Advances in Lithium-Ion Batteries*, Boston, MA: Springer US, 2002, pp. 345–392.

[14] V. A. Sethuraman, L. J. Hardwick, V. Srinivasan, and R. Kostecki, 'Surface structural disordering in graphite upon lithium intercalation/deintercalation', *J. Power Sources*, vol. 195, no. 11, pp. 3655–3660, 2010.

[15] J. Taylor, R. Ball, A. Mcgordon, K. Uddin, and J. Marco, 'Sizing tool for rapid optimisation of pack configuration at early-stage automotive product development', in *Proceedings of the EVS28 International Electric Vehicle Symposium and Exhibition*, pp. 1–8.